Nuclear Materials and Energy 35 (2023) 101420

Contents lists available at ScienceDirect

Nuclear Materials and Energy

journal homepage: www.elsevier.com/locate/nme

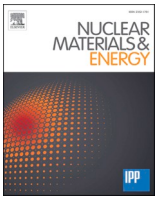

Mechanical and microstructural analysis of tungsten exposed in JET deuterium plasmas

R. Kerr [a,b,*], Y. Zayachuk [b], A. Widdowson [b], E. Alves [c], N. Catarino [c], S. Lozano-Perez [a], D.E.J. Armstrong [a]

[a] Department of Materials, University of Oxford, Parks Road, Oxford OX1 3PH, UK
[b] UK Atomic Energy Authority, Culham Science Centre, Abingdon OX14 3DB, Oxfordshire, UK
[c] IPFN, Instituto Superior Técnico, Universidade de Lisboa, 1049-001 Lisboa, Portugal

A B S T R A C T

A tungsten Langmuir probe exposed in the JET divertor during the ITER-like wall campaigns (ILW) has been studied to evaluate changes in mechanical properties and microstructure. The tip of the probe that was exposed to plasma was cross-sectioned and polished for post mortem analysis. Analysis involved a comparison with a non-exposed probe to determine the effect of plasma exposure on material microstructure and mechanical properties. Visually the probe appeared to have melted and re-solidified during its time in the vessel. Secondary electron (SE) images of cross sections showed the formation of bubbles near the exposed surface that ranged from 50 μm to sub-micron sized. Electron backscatter diffraction (EBSD) revealed that the average grain size had increased from 33 μm to 570 μm. The investigation also showed that hardness had increased from 5.2 to 6.1 GPa and pop-in behaviour was supressed after exposure. This was initially attributed to the uptake of deuterium (D) but nuclear reaction analysis (NRA) indicated that no deuterium remained in the sample and hinted that some other type of defect was modifying the mechanical properties.

1. Introduction

Tungsten has been selected as the main armour material in the ITER divertor and is anticipated to experience quasi-stationary heat loads equivalent to 10–20 MW m^{-2}, transient thermal events of up to 1 GW m^{-2} and an end of life damage level of 1–3 dpa [1–4]. The plasma-facing components in a fusion reactor operating with a deuterium–tritium (DT) fuel mix will be exposed to extreme heat and particle loads. It is the simultaneous application of these damaging interactions that result in unique types of material microstructure which are hard to replicate outside of a reactor environment. Since ITER-relevant reactor conditions are hard to attain, not all fusion material damage is well understood and especially how it affects mechanical and thermal properties. It is important to fully understand these effects in order to predict component lifetimes in both ITER and future devices.

The JET tokamak at the Culham Centre for Fusion Energy is uniquely positioned to address some outstanding questions due to the three ITER-like wall campaigns that ran from 2011–12, 2013–14 and 2015–16. These campaigns employed the same material configuration as ITER, e.g. a beryllium first wall and a tungsten divertor. For this reason it was possible to study the effect of plasma-surface interactions on plasma operation and develop regimes and modelling tools for ITER [5]. The machine was operated with deuterium fuel hence the JET plasma facing components (PFCs) undergo minimal transmutation and neutron damage.

This study consists of a comparison between a non-exposed (as received) Langmuir probe and one that was retrieved from divertor tile 6 at location 26 from divertor module 15 (Fig. 1). Langmuir probes are a type of plasma diagnostic, placed in-between tiles with a tungsten tip which comes into direct contact with the plasma. They are typically used to measure electron temperature, floating potential and ion density in the edge plasma of a tokamak. All JET Langmuir probes were manufactured via sintering and rolling with a tungsten purity greater than 99.95 %.

The exposed probe from tile 6 remained within the JET vessel for two ILW campaigns from 2011 to 2014 and experienced a total of 27.2 h of X-point operation [6]. Gas inventories for injection into the vessel through gas injection modules for 2011–14 are of the order 10^{26} deuterium molecules, 10^{25} hydrogen molecules, 10^{23} ^{4}He + ^{3}He. The number of 2.45 MeV neutrons and 0.82 MeV ^{3}He ions produced by the D-D fusion reaction totalled 2.9×10^{19} for this operating period. Hence, any helium modified microstructure can mainly be attributed to gas injection.

The strike points are the areas in the divertor where the magnetic

* Corresponding author at: Department of Materials, University of Oxford, Parks Road, Oxford OX1 3PH, UK.
E-mail address: robert.kerr@materials.ox.ac.uk (R. Kerr).

https://doi.org/10.1016/j.nme.2023.101420
Received 31 July 2022; Accepted 14 March 2023
Available online 20 March 2023

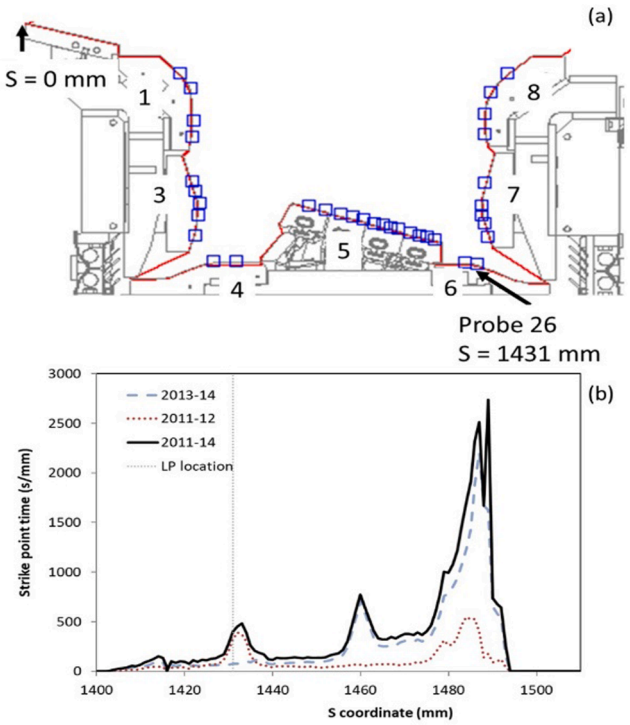

Fig. 1. JET divertor tile configuration during ILW campaigns [6]. Blue squares show the location of Langmuir probes, with probe 26 investigated in this study indicated. S coordinate (millimetres along tile surface) indicated by red line. (For interpretation of the references to colour in this figure legend, the reader is referred to the web version of this article.)

field lines are open onto the tile surface and where the most heat and particles are exhausted from the plasma [7]. The location of the outer strike point (OSP) is detailed in Fig. 1(b) which shows that of the 27.2 h of X-point operation, the OSP was within 10 mm of the probe (s = 1422–1432 mm) for around 0.6 h. Typical ion fluxes to the divertor are $\sim 10^{23}$ D s^{-1} [8], giving a minimum ion fluence of the order $\sim 10^{26}$ ions in this region.

Post mortem analysis was performed and the same characterization techniques were applied to the as received and the tile 6 probes to study the effect of plasma exposure in the JET divertor. The analysis included: Scanning electron microscopy (SEM) to establish areas of interest, electron backscatter diffraction (EBSD) to determine grain size and relate findings to the local crystallographic structure, nanoindentation to measure mechanical properties non-destructively on the micron scale and nuclear reaction analysis (NRA) to map the local retention and distribution of deuterium.

2. Experimental method

Images of a non-exposed and exposed JET Langmuir probes are shown in Fig. 2. The probes are made from solid tungsten and have a tip with a surface area of 8 × 3 mm^2 that is partially exposed to the plasma. Probes are located around the JET divertor and main chamber to cover a full cross section of the vessel. The probe that was investigated in this study was located on tile 6, from the outer divertor, also known as probe 26. It is at the s-coordinate (JET surface coordinate system) s = 1431 mm as shown in Fig. 1.

The triangular probe tip is exposed to plasma and experiences the most extreme conditions. It was cut from the top of the probe body and sectioned to provide two cross-sectional surfaces as indicated in Fig. 2. The sample was prepared for nanoindentation by grinding to a flat surface and adhering to a stainless steel block using *Crystalbond*. The sample was then polished to 1 μm using diamond paste followed by a

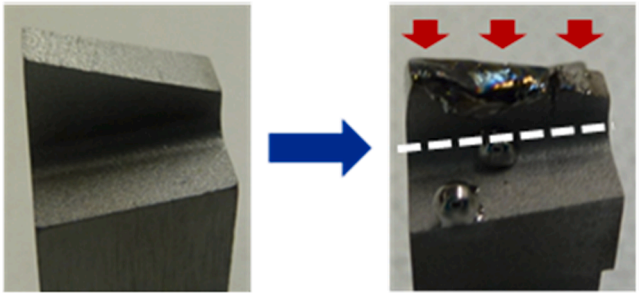

Fig. 2. Optical images of the standard probe tip geometry (left) and the molten probe that was removed for post mortem analysis (right). The red arrows indicate the exposed edge and the dashed line where the tip was cut. (For interpretation of the references to colour in this figure legend, the reader is referred to the web version of this article.)

colloidal silica oxide polishing suspension. The process was repeated for the as received probe, including the sample mounting so the mechanical data from both probes would be directly comparable.

The samples were initially analysed using a TESCAN Mira3 XMH SEM which was equipped with an Oxford Instruments NordlysNano EBSD Detector. SE images were collected to visually compare the microstructure between the probes before and after exposure. EBSD was also used to determine differences in grain size, to relate mechanical data to local crystallographic structure and to help understand the distribution of microstructural features. Grain analysis was carried out using the Oxford Instruments software Aztec where a grain was defined by a continuous boundary with a misorientation of more than 10°.

Mechanical properties were tested in an Agilent G200 nanoindenter. Material hardness as a function of depth was derived from the load–displacement curves for both probes, using the Oliver-Pharr method [9]. The hardness data was obtained in continuous stiffness measurement (CSM) mode, using a diamond Berkovich tip with the area function calibrated on fused silica. The as received probe was indented with an array of 25 indents at a maximum depth of 1 μm and an indent spacing of 25 μm. The spacing was selected to avoid overlapping strain fields and prevent their interactions with GBs which could contribute a hardening effect [10]. However, any indents that were visibly placed near GBs in the SE images were excluded, which left 16 usable indents.

Initially 16 indents were placed in grains with ⟨1 1 1⟩ surface normal direction for the exposed probe. This array had a spacing of 25 μm, a depth of 1 μm and all 16 indents were usable. A further 30 indents were placed in grains with ⟨1 0 1⟩ surface normal, using the same depth and spacing as before. Since these two arrays were placed on the same sample, the compliance of the system should remain consistent and the hardness values can be compared.

In order to obtain mechanical data from local crystallographic grain orientations, the Berkovich indenter tip was exchanged for a spherical tip with a radius of 2 μm. This further simplified data collection since the rotation of the tip did not matter, the residual imprint remained the same for any angle in the plane perpendicular to the surface normal. Spherical tips also enable the full range of elastic–plastic behaviour to be investigated since they create non-self-similar stress fields which causes effective strain to increase with indentation depth [11]. As a result stress–strain curves can be produced without the need for more complicated techniques such as micropillar compression [12].

A common grain orientation in the ⟨1 0 1⟩ direction was selected to indent across both samples to facilitate an accurate comparison. An indentation depth of 1 μm was chosen because the average grain size in the as received probe was 33 μm. A total of 30 indents were placed in each of the samples. An array with a spacing of 15 μm was used for the exposed probe since the size of the indented grain was 705 μm.

Nuclear reaction analysis (NRA) was used to analyse deuterium in the samples using a 2 MeV helium-3 ion beam and the reaction $^{2}H(^{3}He,$

p)^{4}He. The beam was focused to a 10 × 10 × 2 μm spot, extending further into the sample than the depth of the indents performed in this study and this spot was rastered across the sample to create deuterium maps. Scans of the bulk and the exposed edge of the exposed sample cross section were obtained and compared to a control sample containing 4 % deuterium. The limit of detection for deuterium in the exposed probe was derived from the sample containing 4 % deuterium and was found to be 0.02 atomic%.

3. Results and discussion

3.1. Microstructural changes

Fig. 2 shows a significant difference between a probe that remained intact after exposure and the probe that was placed near tile 6 of the JET divertor. Energy-dispersive X-ray spectroscopy (EDX) confirmed that the molten material was tungsten and did not come from elsewhere in the vessel. The appearance of molten tungsten suggests that surface temperatures of the probe exceeded its melting temperature of 3422 °C [13]. These extreme temperatures and resultant melting could have been triggered by a single off-normal event such as transients or a major disruption but have more likely occurred during normal steady-state operation. The assumption being that most major disruptions move in the upward direction away from the divertor. Additionally, the OSP was placed near probe 26 for a considerable amount of time and the probes themselves protrude slightly beyond the boundary of the tiles, hence they are routinely subjected to higher heat loads. In-vessel images taken at the end of the 2011–12 and 2013–14 revealed that the melting occurred during the second ILW operating period. This is consistent with 20 GJ of energy deposited in tile 6 during ILW2 compared with 5.5 GJ of energy in ILW1 [14].

The melt damage that was observed in the optical images, was accompanied by the formation of void-like structures which can be seen in the top half of the sample in Fig. 3. These voids ranged from 50 μm down to sub-micron size which have previously been observed in the TEXTOR tokamak [15]. The voids in the TEXTOR samples were linked to nucleation sites such as impurity clusters or grain boundaries [16] and it was theorised that tungsten evaporation could be involved [17]. Alternatively, void formation in tungsten has also been linked to dopants used in lamp filaments [18] and radiation-induced defects [19] both in the presence of elevated temperatures. Since the amount of helium gas injected into the JET vessel was three orders of magnitude smaller than the amount of deuterium, it is assumed that these voids were not helium bubbles..

If this sample remained in the vessel and was subjected to further heating, these voids/bubbles would likely continue to coalesce and could potentially raise stresses and lead to fracture. Tungsten

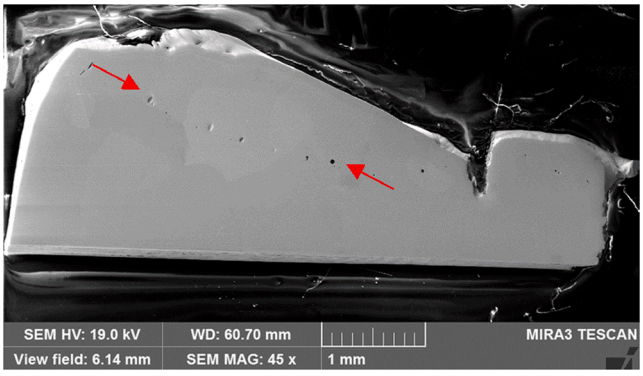

Fig. 3. Secondary electron (SE) image of the tile 6 Langmuir probe that was exposed in the JET divertor. The red arrows indicate the line of voids/bubbles. (For interpretation of the references to colour in this figure legend, the reader is referred to the web version of this article.)

manufacture routes such as sintering and rolling will be used to create components in ITER and other planned devices. It is therefore important to establish in future work whether these voids form as a result of underlying impurities in the as received material or if they stem from defects that are introduced by incident plasma particles.

The EBSD maps in Fig. 4 show that there was a large increase in grain size, from 33 ± 1 μm in the as received sample to 570 ± 60 μm after exposure. This suggests that grain nucleation and growth occurred during re-solidification. These processes are associated with the removal of defects and are typically accompanied by a decrease in mechanical strength and can modify the material's ductile-to-brittle transition temperature, surface roughness and its power handling capabilities [20]. This would be detrimental in a reactor environment where the tungsten PFCs have been specifically engineered to withstand certain conditions.

3.2. Mechanical properties

The hardness values listed in Table 1 were obtained via indentation using a Berkovich tip averaging over a depth of 800–1000 nm. Indentation in the ⟨1 1 1⟩ crystal grain orientation resulted in an increase in hardness of 0.9 GPa, the largest observed increase for the sample. In the ⟨1 0 1⟩ orientation a hardness of 5.7 ± 0.1 GPa and a modulus of 370 ± 10 GPa was measured.

The ⟨1 0 1⟩ grain was positioned closest to the exposed edge, at the top of the sample in Fig. 3 and above the line of voids/bubbles while the ⟨1 1 1⟩ orientation came from the neighbouring grain below the line of voids/bubbles and further away from exposed edge. Interestingly, the harder grain was further below the surface than the region where implantation is expected.

In general it is quite difficult to compare indentation results across multiple studies due to varying system compliance, calibration methods and indent size. The latter causes a phenomenon known as the indentation size effect, where smaller indents record a larger hardness for the same material. This occurs because there are fewer statistically stored dislocations to facilitate material continuity so geometrically necessary dislocations are nucleated under the tip which increases the material flow stress.

These factors are important to consider when comparing experiments that use nanoindentation. A recent study also investigated JET Langmuir probes using a Berkovich nanoindentation but reported a hardness of 5.2 GPa for the exposed tip and 8.5 GPa for the non-exposed probe [21]. This was contrary to the trend that was observed for the tile 6 probe which increased to a hardness of 6.1 GPa from 5.2 GPa in the as received. The majority of studies that have investigated the effect of deuterium plasmas on tungsten in linear plasma devices have reported an increase in hardness due to plasma induced defects [22-24], using a range of indentation depths between 1000 and 2000 nm.

The probe in [21] was retrieved from the vertical inner divertor tile 3 whereas the probe in these experiments came from the base/horizontal divertor tile 6 therefore the difference in hardness can be attributed to the different in-vessel position and therefore plasma exposure. However, the hardness values for the non-exposed probes should be similar between studies. The discrepancy seen here may be related to the different indentation depths used in the two studies; below 200 nm in [21] and between 800 and 1000 nm in this study.

The stress-strain curves in Fig. 5 were obtained via spherical indentation with the assumption that the tip was perfectly spherical. Future work will involve calibrating for the true tip geometry and calculating parameters such as the yield stress and work hardening exponent. The berkovich indents suggest there was a slight decrease in elastic modulus after exposure in JET but the linear elastic region of the stress-strain curves suggest that there has not been a significatn change.

The stress-strain curves also depict the suppression of pop-ins after exposure which can be seen between 2% and 6% strain in Fig. 5. A pop-in is a sudden burst in displacement and is produced when dislocation

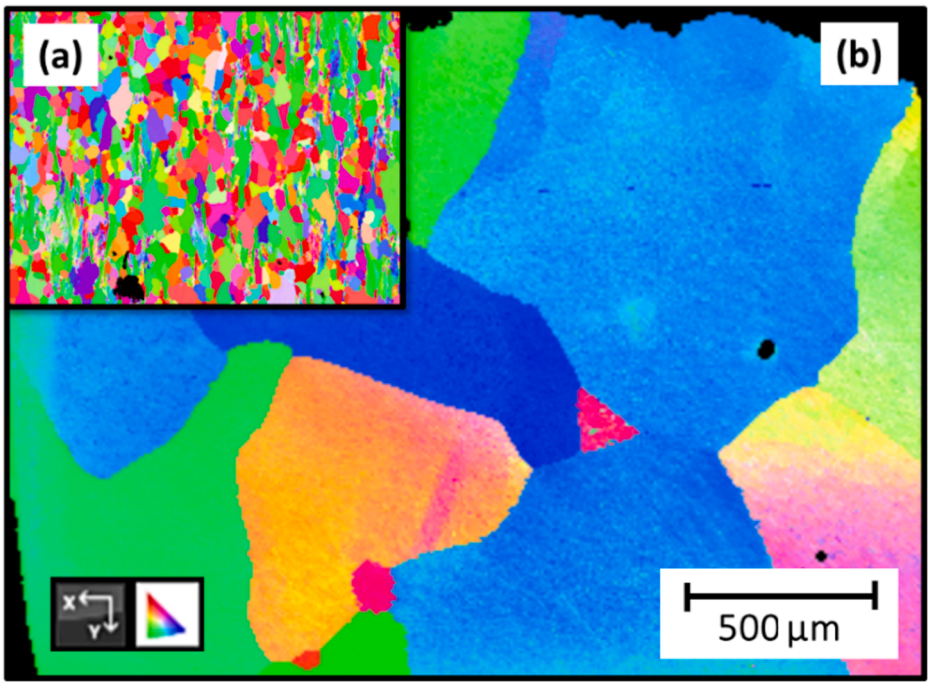

Fig. 4. EBSD images showing the grain size and orientation from (a) The as received Langmuir probe (b) The Langmuir probe that was exposed in the JET divertor.

Table 1
A table depicting how mechanical properties have changed after exposure to JET deuterium plasmas.

	As Received	Tile 6 Probe
Hardness (GPa)	5.2 ± 0.2	6.1 ± 0.1
Modulus (GPa)	390 ± 5	365 ± 5

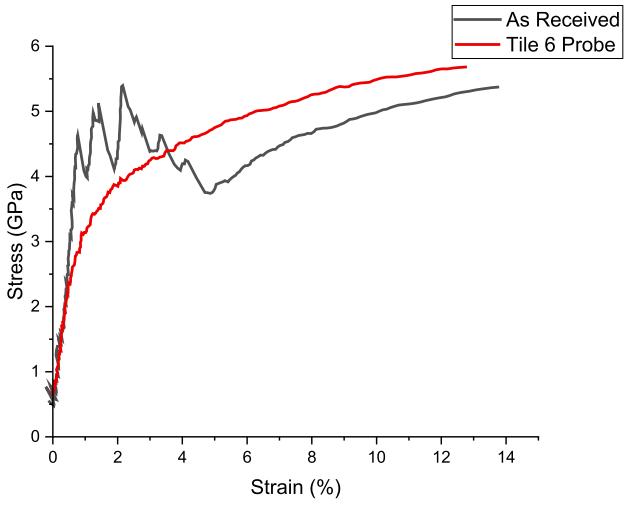

Fig. 5. A stress–strain plot showing the two indents that best represent the overall trends for the as received and tile 6 probe.

sources have been activated that then facilitate plastic deformation. The suppression of pop-ins and the increase in hardness have likely been caused by an increase in defect density. This could ultimately facilitate the nucleation of dislocations and provide obstacles for dislocation motion, resulting in higher stresses.

Deuterium plasmas do not produce nearly as many 14 MeV neutrons and so these defects are unlikely to originate from neutron damage or transmutation. Additionally, the Hall-Petch relation states that material strength decreases with increasing grain size and so this is not the dominant mechanism altering the hardness values [25]. After these results were obtained it was theorised that the hardening of the tile 6 probe could be related the retention of deuterium.

3.3. *Deuterium retention study*

The pop-in behaviours seen in the stress–strain curves could be the result of deuterium present in the sample. In this region, deuterium retention in the tungsten coated – carbon fibre composite divertor tile 6 after exposure 2011–2014 has been shown to be of the order ~ 2–5 × 10^{17} atoms/cm^2 [26]. However, point NRA on the plasma facing surface of the probe shows that deuterium was at the level of 10^{15} atom/cm^2, and is lower in more heavily melted regions, as shown in Fig. 6. Microbeam NRA mapping of the surface and cross section of the sample did not detect the presence of deuterium due to low concentrations. However low concentrations of beryllium and other metallic elements originating from erosion in the vessel were detected. Deuterium levels were assumed to be low either due to outgassing in the vessel during operations, potentially as a result of elevated temperature causing melting, or in the 8 years since removal. Sample preparation using water can also influence the deuterium remaining in the cross sections. This implies that deuterium retention was not the cause of the change in mechanical properties seen in the plasma exposed tile 6 probe.

4. Conclusion

A tungsten Langmuir probe was removed from tile 6 of the JET divertor after the first two ILW campaigns where it had been exposed to deuterium plasmas for a total of 27.2 h. Post mortem analysis was carried out to investigate the effect of plasma exposure on the sample's microstructure and mechanical properties. The findings from this sample were then compared to a reference Langmuir probe which had never been placed inside the vessel. SEM revealed that the tile 6 probe had melted and re-solidified most likely during ILW2 and bubbles had formed near the exposed surface with diameters ranging from the submicron to 50 µm. EBSD indicated that significant grain growth had occurred during the re-solidification process, increasing the grain size

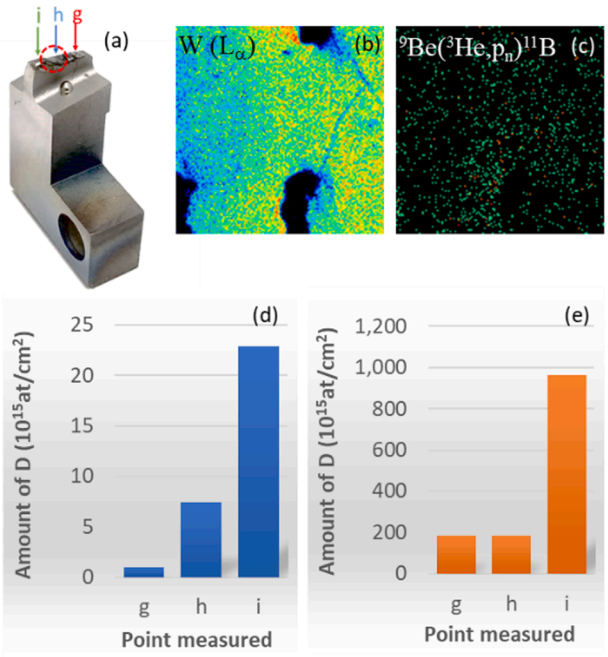

Fig. 6. Micro-beam nuclear reaction analysis mapping and point analysis of surface melted area of exposed tungsten probe.

from 33 μm to 570 μm. Nanoindentation using a Berkovich tip showed that hardness had increased by 0.9 GPa after exposure to JET plasmas. Stress–strain curves produced by spherical nanoindentation showed that pop-in behaviour had also been suppressed. These changes in mechanical properties were thought to be linked to the introduction of plasma-induced defects namely deuterium. NRA confirmed that there was no deuterium present in the cross-section of the tile 6 probe and potentially another type of defect is responsible for the change in mechanical properties.

The changes in microstructure and mechanical properties of the probe represent a history of JET exposure conditions that could also occur in ITER. Tungsten melting is not anticipated in the ITER divertor during steady state operation but may occur during off-normal events. Previous linear fusion device experiments have shown a significant increase in tungsten hardness after exposure to deuterium plasmas. The same trend was observed here, contrary to what is expected after re-solidification and an increase in grain size. The material modifications were attributed to synergistic thermal and plasma effects but the exact mechanism remains unknown. The probe itself would likely be too damaged to withstand the same number of pulses that are planned for the ITER campaigns. Moreover, these campaigns would introduce substantial neutron damage and higher surface temperatures than the ILW campaigns, increasing the probability that a component will fail.

Declaration of Competing Interest

The authors declare that they have no known competing financial interests or personal relationships that could have appeared to influence the work reported in this paper.

Data availability

The data that has been used is confidential.

Acknowledgements

This work has been carried out within the framework of the EUROfusion Consortium, funded by the European Union via the Euratom Research and Training Programme (Grant Agreement No 101052200 — EUROfusion) and from the EPSRC [grant number EP/W006839/1]. To obtain further information on the data and models underlying this paper please contact PublicationsManager@ukaea.uk. Views and opinions expressed are however those of the author(s) only and do not necessarily reflect those of the European Union or the European Commission. Neither the European Union nor the European Commission can be held responsible for them. The research used UKAEA's Materials Research Facility, which has been funded by and is part of the UK's National Nuclear User Facility (NNUF) and Henry Royce Institute for Advanced Materials. The authors also acknowledge the EU H2020 Project No. 824096 "RADIATE" and the support of Luis Alves on microbeam measurements.

References

[1] M. Gago, A. Kreter, B. Unterberg, M. Wirtz, Synergistic effects of particle and transient heat loads on ITER-grade tungsten, Phys. Scr. T171 (2020), 014007, https://doi.org/10.1088/1402-4896/ab3bd9.
[2] R.A. Pitts, et al., Physics basis and design of the ITER plasma-facing components, J. Nucl. Mater. 415 (1 SUPPL) (2011) S957–S964, https://doi.org/10.1016/j.jnucmat.2011.01.114.
[3] T. Cheng, et al., High transient-thermal-shock resistant nanochannel tungsten films, Nanomaterials 11 (10) (2021), https://doi.org/10.3390/nano11102663.
[4] H. Yamada, Nuclear fusion, in: Lackner, M., Sajjadi, B., Chen, W.-Y. (Eds.), Handbook of Climate Change Mitigation and Adaptation, Springer New York, New York, NY, 2020, pp. 1–45.
[5] F. Romanelli, Overview of the JET results, Nucl. Fusion 55 (10) (2015), 104001, https://doi.org/10.1088/0029-5515/55/10/104001.
[6] A. Lahtinen, et al., Deuterium retention in the divertor tiles of JET ITER-Like wall, Nucl. Mater. Energy 12 (2017) 655–661, https://doi.org/10.1016/j.nme.2017.04.007.
[7] S.A. Silburn, et al., Mitigation of divertor heat loads by strike point sweeping in high power JET discharges, Phys. Scr. T170 (2017) 14040, https://doi.org/10.1088/1402-4896/aa8db1.
[8] S. Brezinsek, Plasma-surface interaction in the Be/W environment: conclusions drawn from the JET-ILW for ITER, J. Nucl. Mater. 463 (2015) 11–21, https://doi.org/10.1016/j.jnucmat.2014.12.007.
[9] W.C. Oliver, G.M. Pharr, An improved technique for determining hardness and elastic modulus using load and displacement sensing indentation experiments, J. Mater. Res. 7 (6) (1992) 1564–1583, https://doi.org/10.1557/jmr.1992.1564.
[10] P. Sudharshan Phani, W.C. Oliver, A critical assessment of the effect of indentation spacing on the measurement of hardness and modulus using instrumented indentation testing, Mater. Des. 164 (2019), 107563, https://doi.org/10.1016/j.matdes.2018.107563.
[11] A. Leitner, V. Maier-Kiener, D. Kiener, Essential refinements of spherical nanoindentation protocols for the reliable determination of mechanical flow curves, Mater. Des. 146 (2018) 69–80, https://doi.org/10.1016/j.matdes.2018.03.003.
[12] A.J. Bushby, Nano-indentation using spherical indenters, Nondestruct. Test. Eval. 17 (4–5) (2001) 213–234, https://doi.org/10.1080/10589750108953112.
[13] C. Thomser, et al., Plasma facing materials for the JET ITER-like wall, Fusion Sci. Technol. 62 (1) (2012) 1–8, https://doi.org/10.13182/FST12-A14103.
[14] K. Heinola, et al., Experience on divertor fuel retention after two ITER-Like Wall campaigns, Phys. Scr. T170 (2017) 2017, https://doi.org/10.1088/1402-4896/aa9283.
[15] J.W. Coenen, et al., Analysis of structural changes and high-heat-flux tests on pre-damaged tungsten from tokamak melt experiments, Phys. Scr. T. T145 (2011), https://doi.org/10.1088/0031-8949/2011/T145/014066.
[16] J.W. Coenen, et al., Melt-layer ejection and material changes of three different tungsten materials under high heat-flux conditions in the tokamak edge plasma of TEXTOR, Nucl. Fusion 51 (11) (Nov. 2011) 113020, https://doi.org/10.1088/0029-5515/51/11/113020.
[17] J. W. Coenen et al., "Tungsten melt layer motion and splashing on castellated tungsten surfaces at the tokamak TEXTOR," *J. Nucl. Mater.*, vol. 415, no. 1, pp. S78–S82, Aug. 2011, doi: 10.1016/J.JNUCMAT.2010.09.046.
[18] O. Horacsek, C.L. Toth, K. Horacsek, Void growth mechanism in bubble strengthened tungsten, High Temp. Mater. Process. 13 (1) (1994) 49–60.
[19] I. Ipatova, R.W. Harrison, S.E. Donnelly, M.J.D. Rushton, S.C. Middleburgh, E. Jimenez-Melero, Void evolution in tungsten and tungsten-5wt.% tantalum under in-situ proton irradiation at 800 and 1000 °C, J. Nucl. Mater. 526 (2019) 151730, https://doi.org/10.1016/j.jnucmat.2019.07.030.
[20] A. Suslova, O. El-Atwani, D. Sagapuram, S.S. Harilal, A. Hassanein, Recrystallization and grain growth induced by ELMs-like transient heat loads in deformed tungsten samples, Sci. Rep. 4 (1) (2014) 6845, https://doi.org/10.1038/srep06845.
[21] M. M. Spychalski et al., "Tungsten Langmuir probes from JET-with the ITER-Like Wall: Assessment of mechanical properties by nano-indentation," *Phys. Scr.*, 2021, [Online]. Available: http://iopscience.iop.org/article/10.1088/1402-4896/ac3dbb.

[22] Y. Zayachuk, D.E.J. Armstrong, K. Bystrov, S. Van Boxel, T. Morgan, S.G. Roberts, Nanoindentation study of the combined effects of crystallography, heat treatment and exposure to high-flux deuterium plasma in tungsten, J. Nucl. Mater. 486 (Apr. 2017) 183–190, https://doi.org/10.1016/j.jnucmat.2017.01.026.
[23] X. Fang, et al., Hydrogen embrittlement of tungsten induced by deuterium plasma: Insights from nanoindentation tests, J. Mater. Res. 33 (20) (Oct. 2018) 3530–3536, https://doi.org/10.1557/jmr.2018.305.
[24] D. Terentyev, A. Bakaeva, T. Pardoen, A. Favache, E.E. Zhurkin, Surface hardening induced by high flux plasma in tungsten revealed by nano-indentation, J. Nucl. Mater. 476 (Aug. 2016) 1–4, https://doi.org/10.1016/j.jnucmat.2016.04.007.
[25] S.H. Whang. Introduction," in *Nanostructured Metals and A*, Woodhead Publishing, 2011, pp. xxi–xxxv.
[26] N. Catarino et al., "Deposition in the tungsten divertor during the 2011–2016 campaigns in JET with ITER-like wall," *Phys. Scr.*, vol. T171, p. 014044, Jan. 2020, doi: 10.1088/1402-4896/ab4df7.